Large-model-space calculation of the nuclear level density parameter at finite temperature

B. K. Agrawal and S. K. Samaddar
Saha Institute of Nuclear Physics, 1/AF Bidhannagar, Calcutta 700 064, India

J. N. De
Variable Energy Cyclotron Centre, 1/AF, Bidhannagar, Calcutta 700 064, India

S. Shlomo
Cyclotron Institute, Texas A&M University, College Station, Texas 77841-1366
(Received 26 March 1998)

We calculate the nuclear level density parameter a for a broad range of temperatures ($0.6 \leqslant T \leqslant 6$ MeV) using a microscopic model which includes important ingredients like the thermal and quantal fluctuations of nuclear shapes, continuum corrections, and Coulomb interaction. Numerical calculations have been performed for ^{40}Ca and ^{56}Fe in a large model space. We find that at low temperatures, shell effects are larger for ^{40}Ca and effects of quantal fluctuations are larger for ^{56}Fe. As temperature increases, these effects tend to disappear and continuum corrections become important for $T > 3$ MeV. [S0556-2813(98)04511-7]

PACS number(s): 21.10.Ma, 21.60.−n

The nuclear level density ρ is the basic ingredient required for theoretical studies of nuclear reaction and structure. A simple but useful phenomenological modification of Bethe's formula [1] for ρ leads to the backshifted formula

$$\rho^{\mathrm{BF}} = \frac{\sqrt{\pi}}{12} \frac{e^{2\sqrt{a(E^*-\Delta)}}}{a^{1/4}(E^*-\Delta)^{5/4}} \frac{1}{\sqrt{2\pi\sigma^2}}, \tag{1}$$

in which the pairing effects are mocked up by shifting back the excitation energy E^* by Δ and σ^2 is the spin cutoff factor. The influence of nuclear shell structure, shapes, etc., can be embedded in the the level density parameter a which ultimately leaves a dependent on the excitation energy or temperature (e.g., see Refs. [2–7]).

Recently, there have been several attempts to obtain a realistic dependence of a on temperature in various approaches [3–5,8–12]. Very recently [13], it has been shown that the excitation energy dependence of a obtained in the SPA+RPA approach [12], which includes the thermal fluctuations through static path approximation (SPA) and the quantal fluctuations about static paths using the random-phase approximation (RPA), for medium heavy mass nuclei agrees quite well with the recently available experimental data [14] at low excitation energies. However, the calculations were done for low excitation energies; corrections due to continuum are therefore not included.

In the present work we adopt the SPA+RPA approach, taking into account the effects of the Coulomb interaction and the continuum [3]. We calculate the inverse level density parameter ($K = A/a$) for ^{40}Ca and ^{56}Fe in a large model space over a wide range of temperatures, using SPA as well as SPA+RPA representation of the grand partition function for quadrupole-quadrupole ($\mathbf{Q}\cdot\mathbf{Q}$) interaction model Hamiltonian. Effects of quantal fluctuations as well as continuum corrections are studied.

Let us start with the $\mathbf{Q}\cdot\mathbf{Q}$ Hamiltonian

$$H = H_0 - \frac{1}{2}\chi \sum_{\mu=-2}^{2} (Q_\mu)^2. \tag{2}$$

Here, H_0 represents the spherical part, $Q_0 = Q_0'$, $Q_{+\mu} = 1/\sqrt{2}(Q_\mu' + Q'^{\dagger}_{\mu})$ and $Q_{-\mu} = i/\sqrt{2}(Q_\mu' - Q'^{\dagger}_{\mu})$ with $\mu = 1$ and 2 and $Q's$ stand for the usual quadrupole moment operators. The value of the quadrupole interaction strength

$$\chi = 120 A^{-5/3} f_c \ \text{MeV} \tag{3}$$

(A denotes the mass number) is taken from Ref. [15] where f_c is a core polarization factor. The partition function is then written as

$$\mathcal{Z} = \mathcal{Z}_c^{-1} \left\{ 4\pi^2 \left(\frac{\alpha}{2\pi T} \right)^{5/2} \times \int \beta^4 d\beta \int |\sin 3\gamma| d\gamma e^{-\alpha\beta^2/2T} \mathrm{Tr}[e^{-H'/T}] \mathcal{C}_{\mathrm{RPA}} \right\}, \tag{4}$$

where, the quantity within braces represents the SPA+RPA representation of the grand partition function with $\alpha = (\hbar\omega_0)^2/\chi$ and $\hbar\omega_0 = 41 A^{-1/3}$ MeV. The single-particle Hamiltonian H' and the RPA correction factor $\mathcal{C}_{\mathrm{RPA}}$ are given as

$$H' = H_0 - \hbar\omega_0 \beta (Q_0 \cos\gamma + Q_{+2} \sin\gamma) \tag{5}$$

and

$$\mathcal{C}_{\mathrm{RPA}} = \left[\prod_{m\neq 0}^{N_m} \mathrm{Det}|C^m| \right]^{-1}, \tag{6}$$

respectively, with

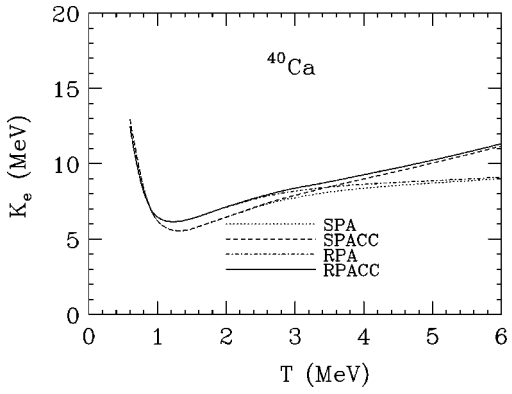

FIG. 1. Variation of the inverse level density parameter K_e $(=A/a_e)$ with temperature for ^{40}Ca. Dotted and dashed curves as labeled by SPA and SPACC correspond to the SPA results without and with continuum corrections, respectively. Dash-dot and full lines represent RPA results without and with continuum corrections, respectively.

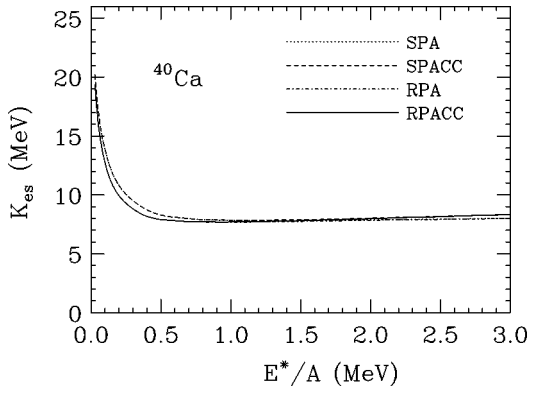

FIG. 2. Variation of the inverse level density parameter K_{es} $(=A/a_{es})$ with E^*/A for ^{40}Ca. The curves labeled SPA, SPACC, RPA, and RPACC have a similar meaning to those in Fig. 1.

$$C^m_{\mu\nu}=\delta_{\mu\nu}+\chi\sum_{ij}\frac{\langle i|Q_\mu|j\rangle\langle j|Q_\nu|i\rangle}{\Delta_{ij}^2+(2\pi mT)^2}f_{ij}\Delta_{ij}. \tag{7}$$

Here, $f_{ij}=f_i-f_j$ and $\Delta_{ij}=\epsilon_i-\epsilon_j$ with f_i being the Fermi distribution function and ϵ_i is the eigenvalue of H'. In the above, $|i\rangle$ represents an eigenstate of H'. The grand canonical trace in Eq. (4) can be performed using

$$\mathrm{Tr}\,e^{-\beta' H'}=\left(\prod_i\,[1+e^{-\beta'\epsilon_i+\alpha_p}]\right)\left(\prod_j\,[1+e^{-\beta'\epsilon_j+\alpha_n}]\right), \tag{8}$$

where, $\beta'=1/T$ and $\alpha_p(\alpha_n)$ is the Lagrange multiplier required to adjust the proton (neutron) numbers.

The SPA representation of the partition function can be obtained by putting $\mathcal{C}_{\mathrm{RPA}}=1$. It is clear from Eqs. (6) and (7) that for higher temperatures $\mathcal{C}_{\mathrm{RPA}}\to 1$ (and $\mathcal{Z}\to\mathcal{Z}_{\mathrm{SPA}}$).

The coefficient $\mathcal{Z}_c^{-1}$ [appearing in Eq. (4)] which represents continuum corrections [3–5] is obtained as

$$\mathcal{Z}_c=\left(\prod_i\,[1+e^{-\beta'\epsilon_i^c+\alpha_p}]\right)\left(\prod_j\,[1+e^{-\beta'\epsilon_j^c+\alpha_n}]\right), \tag{9}$$

where, ϵ_i^c and ϵ_j^c are the single-particle energies in the continuum for protons and neutrons, respectively, as discussed in the next section. Once the partition function is known, the average number of particles (N), energy (E), and entropy (S) at a fixed temperature can be obtained using the thermodynamical relations,

$$N_{p,n}=\frac{\partial\ln\mathcal{Z}}{\partial\alpha_{p,n}}, \tag{10}$$

$$E=-\frac{\partial\ln\mathcal{Z}}{\partial\beta'}, \tag{11}$$

$$S=\ln\mathcal{Z}+\beta' E-\alpha_p N_p-\alpha_n N_n. \tag{12}$$

Now using Eqs. (10), (11), and (12) we can determine the level density parameter a as follows:

$$E^*=a_e T^2, \tag{13}$$

$$S=2a_s T, \tag{14}$$

$$S^2=4a_{es}E^*. \tag{15}$$

Since in general the level density parameter depends on temperature, its values obtained using Eqs. (13) and (14) are different. However, the parameter $a_{es}=a_s^2/a_e$ [Eq. (15)] should only be used in the Bethe level density formula [5,6,13].

The basis states are taken to be the eigenstates of H_0 having the form

$$H_0=\frac{p^2}{2m}+V_0 f(r)+V_{ls}g(r)+\eta V_C, \tag{16}$$

where, p and m represent the momentum and mass of the nucleon, respectively. The r dependence in the second term is taken to be

$$f(r)=\begin{cases}\dfrac{V_0}{1+e^{(r-R)/d}} & \text{for } r\leqslant R_{\max}\\ +\infty & \text{for } r>R_{\max},\end{cases} \tag{17}$$

where $R=r_0A^{1/3}$ is the nuclear radius, d the diffuseness parameter, and $R_{\max}=R+2\pi d$ as is considered in Ref. [3]. We adopt the Thomas form factor

$$g(r)=\begin{cases}\dfrac{r_0^2}{r}\dfrac{d}{dr}f(r) & \text{for } r\leqslant R_{\max}\\ 0 & \text{for } r>R_{\max}\end{cases} \tag{18}$$

and the strength

$$V_{ls}=\begin{cases}-(l+1)V_{ls}^0 & \text{for } j=l-\dfrac{1}{2}\\ lV_{ls}^0 & \text{for } j=l+\dfrac{1}{2},\end{cases} \tag{19}$$

where, l and j represent the orbital and total angular momentum quantum number for the single-particle basis states. In the last term of Eq. (16), $\eta=0$ (1) for neutron (proton) and

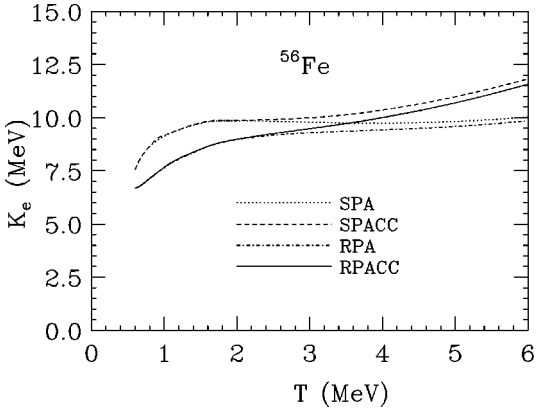

FIG. 3. Same as Fig. 1 but for ^{56}Fe.

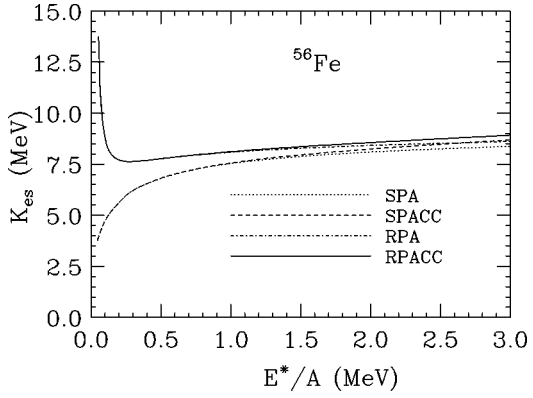

FIG. 4. Same as Fig. 2 but for ^{56}Fe.

V_C is the Coulomb potential associated with a uniformly charged sphere of radius $R_c = r_c A^{1/3}$. The value of the potential parameters used in Eq. (16) are $V_0 = -53.0$ MeV, $V_{ls}^0 = 8.5$ MeV, $d = 0.65$ fm, $r_0 = 1.25$ fm, and $r_c = 1.30$ fm.

The model space spans all the single-particle states with quantum number $0 \leqslant N \leqslant 6$ where $N = 2n + l$, n being the principle quantum number. This corresponds to single-particle states with energies up to around 35 MeV above the Fermi energy. Our results for the level density parameter are therefore expected to be quite reliable for temperatures as high as the limiting temperature (≈ 6 MeV). We use these basis states to perform also a mean-field calculation for the $\mathbf{Q}\cdot\mathbf{Q}$ Hamiltonian given by Eq. (2) and find that the ground-state deformation of ^{40}Ca as well as ^{56}Fe agree fairly well with the observed ones when f_c in Eq. (3) is taken to be 0.75. The values of ϵ^c [see Eq. (9)] can be calculated by solving the Schrödinger equation with the nuclear interaction in Eq. (16) switched off using the boundary condition that the wave function vanishes beyond $R_{\max}$.

In Fig. 1 we display the variation of $K_e (= A/a_e)$ as a function of temperature obtained for ^{40}Ca using SPA and SPA+RPA approaches with and without inclusion of the continuum corrections (CC). In the following discussions we shall refer to SPA+RPA simply by RPA and use CC if continuum corrections are included. We see that for $T < 1.5$ MeV, the parameter K_e is very large and decreases rapidly with temperature. These large values of K_e (or smaller a_e) at very low temperature are due to the shell closure. For $T > 1.5$ MeV when shell effects are expected to vanish, values of K_e for ^{40}Ca and ^{56}Fe (see Fig. 3) become closer. Another important point we note is that the effects of quantal fluctuations are not very significant even at very low temperatures. For $T > 1.5$ MeV, K_e increases monotonically. The values of K_e become slightly larger for $T > 3$ MeV when continuum corrections are included.

In Fig. 2, the variation of $K_{es} (= A/a_{es})$ with E^*/A (excitation energy per nucleon) for ^{40}Ca is shown. The values of K_{es} also show large variation at low E^*/A (or temperature). For $E^*/A > 0.35$ MeV (or $T > 1.5$ MeV), K_{es} increases slowly with E^*/A. However, the rate of increase as well as the effect of continuum corrections at higher E^*/A is smaller for K_{es} than in the case of K_e.

In Figs. 3 and 4, the results for K_e and K_{es} obtained for ^{56}Fe are displayed. Once again, as seen for ^{40}Ca, we see from Figs. 3 and 4 that the SPA (dotted) and the RPA (dash-dot) results for ^{56}Fe show a rapid variation of $K_e (K_{es})$ with $T (E^*/A)$ for $T < 1.0$ MeV ($E^*/A < 0.3$ MeV). However, in the SPA, the value of K_e increases whereas in the RPA, the results show the opposite trend. This difference is caused by the inclusion of the quantal fluctuation effects in the RPA approach. We would like to mention here that in the case of ^{40}Ca (Figs. 1 and 2), the RPA effects seem to be quite a bit smaller compared to that for ^{56}Fe. The reason for this is as follows. Looking at Eqs. (6) and (7) and the single-particle spectrum, we find that the maximum contribution to $\mathcal{C}_{\rm RPA}$ for ^{56}Fe comes from closely lying p and f states near the Fermi surface. On the other hand, in the case of ^{40}Ca, the contribution to $\mathcal{C}_{\rm RPA}$ comes from the $0d$ and $0g$ states which are lying far apart in energy. As temperature increases, the RPA effects become less significant. For $T > 1$ MeV, the SPA as well as the RPA results show slow monotonic increase of K_e as well as K_{es} with T (or E^*/A). The continuum corrections to the value of K_e and K_{es} (seen from the label SPACC and RPACC) are insignificant for the $T < 3$ MeV. For $T > 3$ MeV, however, K increases faster with the inclusion of continuum corrections. It may be interesting to point out that the present results for $T > 1$ MeV depict similar trends as that found in Ref. [4] for the $A = 160$ mass region.

In Fig. 5 we compare K_e with K_{es} for ^{40}Ca (upper panel) and ^{56}Fe (lower panel) obtained using RPACC. We see that in general, values of K_e differ significantly from K_{es} at a fixed temperature. It is interesting to note that when the

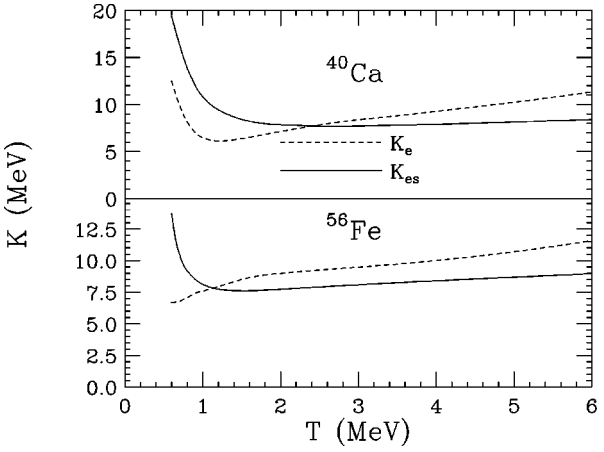

FIG. 5. Comparison of K_e and K_{es} at fixed temperatures for ^{40}Ca and ^{56}Fe.

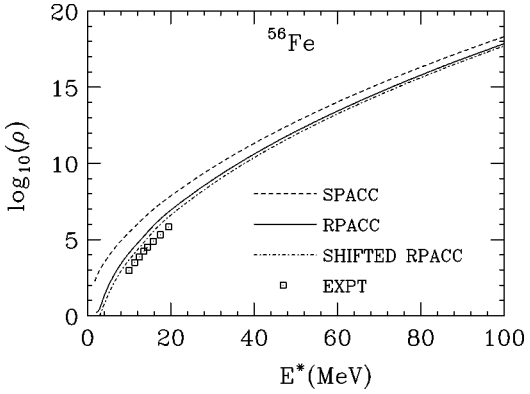

FIG. 6. Variation of the total level density as a function of E^* for ^{56}Fe. The dashed and full curves are obtained using SPACC and RPACC values for K_{es} in the Bethe's formula (1) with $\Delta=0$. The dash-dot curve represents RPACC results obtained using $\Delta=1.38$ MeV.

variation of K_e with temperature is large, the difference between K_e and K_{es} is also large. Exploiting the thermodynamic relation

$$\frac{dS}{dE}=\frac{1}{T}, \tag{20}$$

one finds that if $dK_e/dT=0$, then only one would have $K_e=K_{es}$ (or $a_e=a_{es}$).

For a light doubly closed-shell nucleus like ^{40}Ca, pairing is expected to be small. In Ref. [16], the contribution of pairing to the level density parameter is reported to be very significant for ^{40}Ca; however, their calculated level density parameter with inclusion of pairing overestimates the experimental value. On the other hand, for the nucleus ^{56}Fe Nakada and Alhassid [17] find that the effect of pairing on level density can be simulated through a backshift in the excitation energy which is $\Delta=1.38$ MeV. We have also followed this prescription. In Fig. 6, the variation of the total level density $\rho(E^*)$ as a function of E^* for ^{56}Fe is shown. We calculate $\rho(E^*)$ by using in Eq. (1) the values of the level density parameter obtained using SPACC and RPACC. The dashed and full lines are obtained with $\Delta=0$ (no back shift) and dash-dot is obtained with $\Delta=1.38$ MeV in Eq. (1). The experimental data [14] available for $10<E^*<20$ MeV are also shown as squares. One finds that the RPACC results show reasonable agreement with the observed ones, whereas, the SPACC results overestimate the values of $\rho(E^*)$ as already seen in Ref. [13].

This work was supported in part by the U.S. National Science Foundation under Grant No. PHY-9413872.

[1] A. Bohr and B. Mottelson, *Nuclear Structure* (Benjamin, Reading, MA, 1969), Vol. I.
[2] S. K. Kataria, V. S. Ramamurthy, and S. S. Kapoor, Phys. Rev. C **18**, 549 (1978).
[3] S. Shlomo and J. B. Natowitz, Phys. Lett. B **252**, 187 (1990).
[4] S. Shlomo and J. B. Natowitz, Phys. Rev. C **44**, 2878 (1991).
[5] J. N. De, S. Shlomo, and S. K. Samaddar, Phys. Rev. C **57**, 1398 (1998).
[6] J. P. Lestone, Phys. Rev. C **52**, 1118 (1995).
[7] B. K. Agrawal and A. Ansari, Phys. Lett. B **339**, 7 (1994).
[8] S. Shlomo, Nucl. Phys. **A539**, 17 (1992).
[9] S. Shlomo, V. M. Kolomietz, and H. Dejbakhsh, Phys. Rev. C **55**, 1972 (1997).
[10] G. H. Lang, C. W. Johnson, S. E. Koonin, and W. E. Ormand, Phys. Rev. C **48**, 1518 (1993), and references therein.
[11] S. E. Koonin, D. J. Dean, and K. Langanke, Phys. Rep. **278**, 1 (1997).
[12] G. Puddu, P. F. Bortignon, and R. A. Broglia, Ann. Phys. (San Diego) **206**, 409 (1991).
[13] B. K. Agrawal and A. Ansari, Phys. Lett. B **421**, 13 (1998).
[14] D. R. Chakrabarty, V. M. Datar, Suresh Kumar, T. Mirgule, H. Oza, and U. K. Pal, Phys. Rev. C **51**, 2942 (1995).
[15] S. Aberg, Phys. Lett. B **157**, 9 (1985).
[16] C. Gregoire, T. T. S. Kuo, and D. B. Stout, Nucl. Phys. **A530**, 94 (1991).
[17] H. Nakada and Y. Alhassid, Phys. Rev. Lett. **79**, 2939 (1997).